Crashworthiness design of density-graded cellular metals

Xiaokai Wang, Zhijun Zheng,[a] and Jilin Yu
CAS Key Laboratory of Mechanical Behavior and Design of Materials, University of Science and Technology of China, Hefei 230026, China

(Received 13 March 2013; accepted 15 April 2013; published online 10 May 2013)

Abstract Crashworthiness of cellular metals with a linear density gradient was analyzed by using cell-based finite element models and shock models. Mechanisms of energy absorption and deformation of graded cellular metals were explored by shock wave propagation analysis. Results show that a positive density gradient is a good choice for protecting the impacting object because it can meet the crashworthiness requirements of high energy absorption, stable impact resistance and low peak stress. [doi:10.1063/2.1303101]

Keywords functionally graded materials, deformation localization, shock model, crashworthiness

Cellular metals have considerable capacity in energy absorption and mitigation of impact/blast loads.[1,2] They are widely used as crashworthiness structures in the automotive, railway and aeronautical industries. The quasi-static stress–strain curve of a cellular metal with a uniform density usually has a long plateau stage stably absorbing energy.[3] Under intense loads, cellular metals undergo large plastic deformation as sacrificial claddings for object protection. Strength enhancement is found in the response of cellular metals to dynamic loadings, which has been well explained by the one-dimensional shock models.[4–7] Shock wave propagation in cellular metals is affected by changing the local material properties,[8] and therefore introducing a density gradient to cellular metals may help to improve their crashworthiness.

Graded cellular metals (GCMs) with a gradual change in mechanical properties of their constituent phases have been proposed in the open literature.[8,9] The manufacture of GCMs is full of challenges, especially with specific functions. Brothers and Dunand[10] provided an investment casting method based on replication of density-graded polymer foams to create density-graded open-cell aluminum foam. Besides, Hangai et al.[11] fabricated density-graded closed-cell aluminum foam with a varying pore distribution by using high-pressure die castings containing a large amount of gas. As the material design of GCMs is available, it is desirable to understand their functional design principles.

In the crashworthiness design, energy absorption and impact resistance are two design objectives.[12] The present study aims to design GCMs with functions to meet the requirement of crashworthiness for protecting the impacting object. The mechanisms of energy absorption and impact resistance for the GCMs used are explained by cell-based finite element (FE) models and shock models.

Consider a mass M traveling with an initial velocity V_0. A stationary cellular rod with a uniform density ρ_0 and a cross-sectional area A_0 is used to stop the mass, see Fig. 1(a) for the schematic diagram. It is easy to design the length of the rod when using the well-known RPPL (rigid-perfectly plastic-locking) shock model, which was firstly proposed by Reid and Peng[4] and further developed by many authors.[5–7] Assuming a single plastic shock front propagates along the rod, Reid et al.[4,5] determined the shock-enhanced stress as

$$\sigma_{\mathrm{B}} = \sigma_0 + \rho_0 v^2/\varepsilon_{\mathrm{L}}, \tag{1}$$

where v is the velocity of the mass, σ_0 is the plateau stress (or yield stress, used later) and ε_{L} is the locking strain in the RPPL idealization. The explicit solution of velocity $v(t)$ was recently obtained by Zheng et al.,[6,7] written as

$$v(t) = V_0\,(1 - t/T)\left[1 + \alpha - \alpha(1 - t/T)^2\right]^{-1/2}, \tag{2}$$

where t is the time, $\alpha = \rho_0 V_0^2/(\sigma_0\varepsilon_{\mathrm{L}})$ is the initial shock-enhancement parameter and $T = MV_0/(\sigma_0 A_0)$ is the characteristic time parameter corresponding to $v(T) = 0$. Considering the case that the cellular rod is just fully crushed when the input kinetic energy is exhausted, we can design the length of the rod as

$$L = \Phi(T) = \left(\sqrt{1+\alpha} - 1\right) m/\rho_0, \tag{3}$$

where $\Phi(t) = \int_0^t v(t)\,\mathrm{d}t/\varepsilon_{\mathrm{L}}$ is the Lagrangian location of the shock front and $m = M/A_0$.

Instead of a uniform density distribution of the cellular rod, we use a linear density distribution along the rod (X axis) to improve the design. The length and the average density of the cellular rods are considered to be unchanged. The density distribution of a graded cellular rod is given by

$$\rho_{\mathrm{f}}(X) = \rho_0\left[1 + \gamma\,(X/L - 1/2)\right], \tag{4}$$

where γ is the density-gradient parameter and ρ_0 is the average density of the graded cellular rod. For $\gamma < 0$, the density linearly decreases along the rod, and for $\gamma > 0$, the density linearly increases along the rod. We will employ numerical and theoretical methods to determine the appropriate value of the density-gradient parameter.

[a] Corresponding author. Email: zjzheng@ustc.edu.cn.

The numerical method is based on the cell-based FE models and the theoretical method is based on the shock models.

The cell-based FE models of GCMs are constructed with the varying cell-size distribution method.[8] The two-dimensional (2D) Voronoi technique[13] with a new principle of seeding nuclei is used to generate cellular samples. Nuclei are randomly seeded by the principle that the distance between any two nuclei i and j is not less than the minimum allowable distance[8]

$$\delta_{ij}^{\min} = (1-k)\cdot 2\rho_{\rm s}h/\rho_{\rm f}[(X_i+X_j)/2], \tag{5}$$

where h is the specified cell-wall thickness, $\rho_{\rm s}$ is the density of cell-wall solid, k is the cell irregularity, and (X_i, Y_i) is the location of nucleus i. In this study, $\rho_0/\rho_{\rm s} = 0.1$, $k = 0.2$, $h = 0.26$ mm and $\rho_{\rm s} = 2\,700$ kg/m^3. Three samples with length $L = 383$ mm and width $W = 100$ mm for $\gamma = 0$, -1, 1 are shown in Figs. 1(a), 1(b), 1(c), respectively. GCM specimens with thickness $H = 1$ mm are thus obtained. The length of the specimens is determined from Eq. (3) for $M = 5$ g and $V_0 = 120$ m/s. Impact tests of GCM specimens are performed by using FE method with ABAQUS/Explicit code. The cell-wall material of cellular metals is taken to be elastic-perfectly plastic with Young's modulus, Possion's ratio and yield stress being $E = 69$ GPa, $\nu = 0.3$ and $\sigma_{\rm y} = 170$ MPa, respectively. Cell walls are modeled with shell elements of type S4R. Any possible contact surfaces are defined in contact with slight friction, as done in Refs. 8 and 13.

Deformation patterns for three kinds of GCM specimens at $t = 2$, 4, 6 ms are shown in Fig. 1. For $\gamma = 0$ in Fig. 1(a), cells closed to the impact end of the specimen are crushed progressively and a deformation band like a structural shock wave propagates towards the support end. For $\gamma = 1$ in Fig. 1(c), the deformation process is similar to that of $\gamma = 0$, but cells are crushed in a much narrow band. For $\gamma = -1$ in Fig. 1(b), it is interesting to observe that, besides the deformation band closed to the impact end, another deformation band appears near the support end and propagates in an opposite direction.

The nominal stress–time curves at the impact and support ends of GCM specimens with $\gamma = 0$, -1, 1 are shown in Fig. 2. Hereinafter, the stresses at the two ends of a specimen are referred as the impact stress and the support stress, respectively. For $\gamma = 0$ in Fig. 2(a), the impact stress (ignoring the oscillation) drops rapidly at the initial stage and then decreases gradually with the increasing time, but the support stress is much stable before 5 ms and increases after 5 ms due to the wave reflection at the support end. For $\gamma = -1$ in Fig. 2(b), the impact stress drops rapidly to zero at the initial stage and then increases gradually with the increasing time, and the support stress increases gradually before the end of impact. For $\gamma = 1$ in Fig. 2(c), the impact stress decreases and the support stress increases gradually with the increasing time, and its total impact time (6.02 ms) is much less than those of $\gamma = 0$ and -1.

The one-dimensional shock models well explain the deformation features of uniform cellular metals under dynamic loading.[4–7] Here, we extend the RPPL shock model for GCMs to explain their deformation features. It should be noted that the local strength in a GCM specimen depends on the local density. The material parameters for the RPPL idealizations with different densities are fitted with $\sigma_0/\sigma_{\rm y} = c\rho^2$ and $\varepsilon_{\rm L} = \varepsilon_{\rm D} = r(1-\rho)$, where $\rho = \rho_{\rm f}/\rho_{\rm s}$ is the relative density and $\varepsilon_{\rm D}$ is the densification strain of cellular metals.[3] Here, $c = 0.417$ and $r = 0.725$.

For $\gamma = 0$, the shock-enhanced stress and the impact velocity predicted by the RPPL shock model have been given in Eqs. (1) and (2), respectively. Thus, the impact stress can be determined as $\sigma_{\rm i} = -m\,{\rm d}v/\,{\rm d}t$ by using the inertial law. The support stress is given by $\sigma_{\rm s} = \sigma_0(\rho_0/\rho_{\rm s})$. These predicted stresses are compared reasonably well with the FE results, except for the support stress when $t > 5$ ms, see Fig. 2(a). Improving the idealization of the cellular metals might improve the predictions,[6,7] but it is beyond the scope of this paper.

For $\gamma > 0$, the shock wave propagation is similar to that of $\gamma = 0$. Thus, the RPPL shock model is easy to be extended for this case. The main difference is due to that the two material parameters σ_0 and $\varepsilon_{\rm D}$ are related to the local relative density in a GCM specimen. By using the kinematic and kinetic compatibility conditions across the shock front, the shock speed and the shock-enhanced stress can be given by

$$\dot{\Phi} = v/\varepsilon_{\rm D}(\rho(\Phi)), \tag{6}$$

and

$$\sigma_{\rm B} = \sigma_0(\rho(\Phi)) + \rho_{\rm f}(\Phi)v^2/\varepsilon_{\rm D}(\rho(\Phi)), \tag{7}$$

respectively. The inertial law of the mass together with the deformed portion of the specimen gives

$$\frac{{\rm d}v}{{\rm d}t} = -\sigma_{\rm B}\left(m + \int_0^{\Phi}\rho_{\rm f}(X)\,{\rm d}X\right)^{-1}. \tag{8}$$

Combining Eqs. (6) and (8) leads to a second-order differential equation of $\Phi(t)$, but its solution could not be obtained explicitly. Instead, we used a numerical method, e.g. the Runge–Kutta algorithm, to solve Eqs. (6) and (8) with the initial conditions $\Phi(0) = 0$ and $v(0) = V_0$. The impact stress is also determined from $\sigma_{\rm i} = -m\,{\rm d}v/\,{\rm d}t$ and the support stress is obtained by $\sigma_{\rm s} = \sigma_0(\rho(\Phi))$. The predicted stresses for $\gamma = 1$ are shown in Fig. 2(c). The impact stress drops gradually and the support stress increases gradually during the impact process in this case. However, when γ is large enough, e.g., $\gamma = 1.5$ in Fig. 2(d), the impact stress firstly increases and then decreases with the increase of the time.

For $\gamma < 0$, two shock waves are formed at the two ends of the GCM specimen. Similar work using the extended RPPL shock model for GCMs has been considered in the literature.[14] However, in Ref. 14 the authors

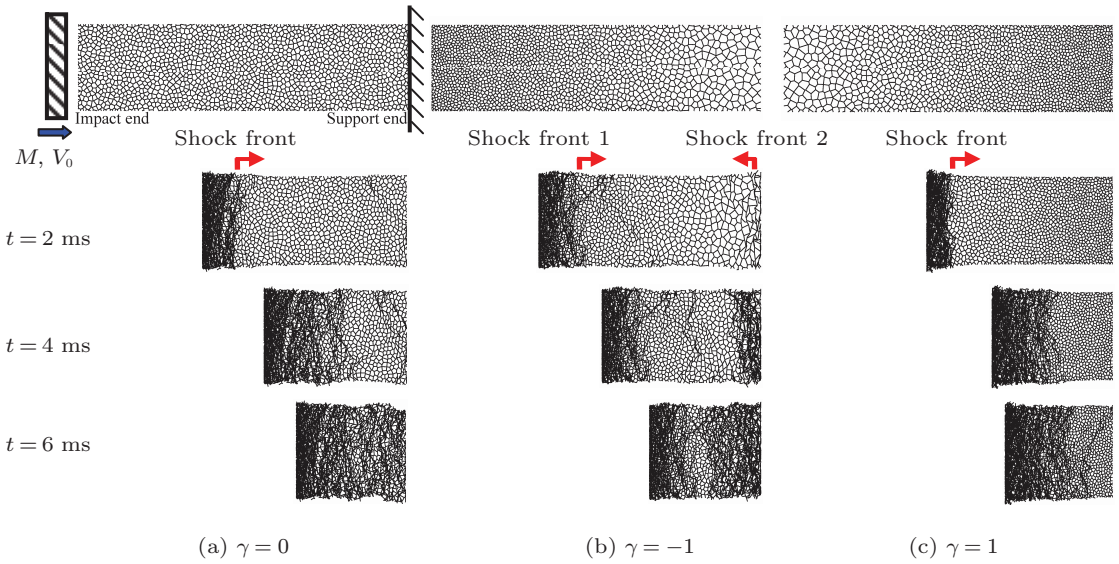

Fig. 1. Finite element models and deformation patterns of cellular metals with density-gradient parameters (a) $\gamma = 0$, (b) $\gamma = -1$, (c) $\gamma = 1$ when $M = 5$ g and $V_0 = 120$ m/s.

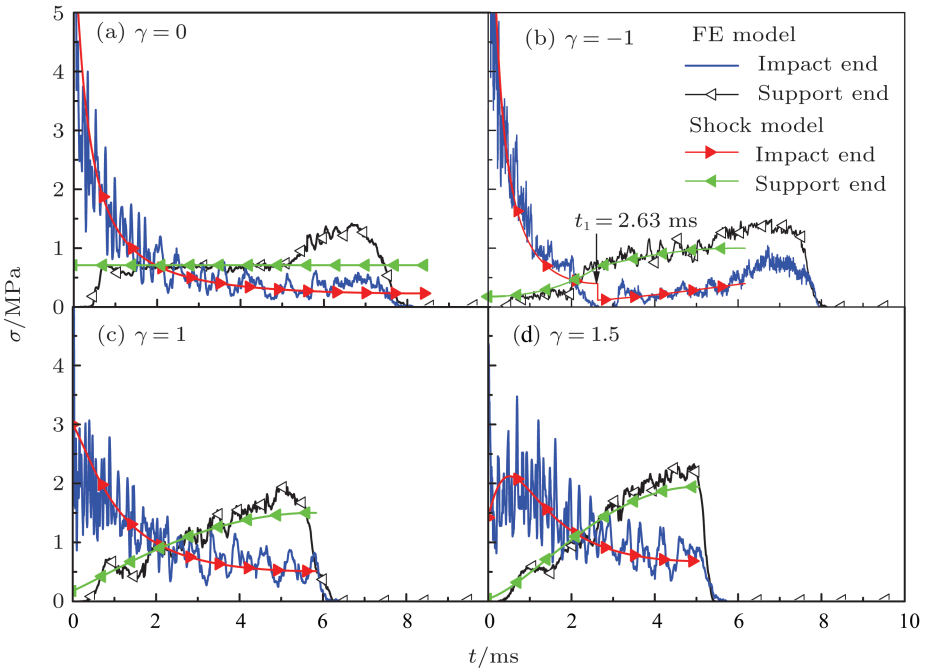

Fig. 2. Comparisons between the results of numerical simulations and the predictions using the shock models for GCMs with (a) $\gamma = 0$, (b) $\gamma = -1$, (c) $\gamma = 1$, (d) $\gamma = 1.5$.

considered the specimen with a strength gradient but not a density gradient. Below we outline the extended RPPL shock model for the case of $\gamma < 0$.

At time t, the two shock fronts locate at Φ_1 and Φ_2 in the Lagrangian coordinate, respectively. The undeformed region between the two shock fronts ($\Phi_1 < X < \Phi_2$) travels with velocity v_u, the particle acceleration in this region should be consistent, which can be written as

$$a(t) = -\frac{1}{\rho_f(X)}\frac{\mathrm{d}\bar{\sigma}(X)}{\mathrm{d}X}, \tag{9}$$

where $\bar{\sigma}(X)$ is the stress distribution in the undeformed region ($\Phi_1(t) < X < \Phi_2(t)$). Integrating Eq. (9) with Eq. (4), we have the stress distribution in the undeformed region

$$\bar{\sigma}(X) = \bar{\sigma}(\Phi_2) - a(t)\int_X^{\Phi_2} \rho_f(\zeta)\,\mathrm{d}\zeta =$$

$$\frac{a(t)\rho_0 L}{2\gamma}[1+\gamma\,(X/L-1/2)]^2+\bar{\sigma}(\Phi_2)-\frac{a(t)\rho_0 L}{2\gamma}[1+\gamma\,(\Phi_2/L-1/2)]^2, \tag{10}$$

but $\bar{\sigma}(\Phi_2)$ is undetermined. In the undeformed region of the specimen, the stress $\bar{\sigma}(X)$ should not be larger than the local yield stress $\sigma_0(\rho(X)/\rho_s)$, which gives

$$\bar{\sigma}(X)\leqslant\sigma_y c\,(\rho_0/\rho_s)^2\,[1+\gamma\,(X/L-1/2)]^2 \tag{11}$$

for any X ranging from Φ_1 to Φ_2. It is easy to find that Eq. (11) can always take an equal sign when taking $\bar{\sigma}(\Phi_2)=\sigma_0(\rho(\Phi_2)/\rho_s)$ and

$$a(t)=-\frac{2\gamma c\rho_0\sigma_y}{\rho_s^2 L}\equiv a_0. \tag{12}$$

This means that the stress in the undeformed region can reach its local yield stress for the specific case of density distribution considered. And thus, $v_u=a_0 t$. Using the kinematic and kinetic compatibility conditions across shock-front 1 (close to the impact end) and across shock-front 2 (close to the support end), we obtain the shock speeds

$$\begin{aligned}\dot{\Phi}_1&=(v-v_u)/\varepsilon_D(\rho(\Phi_1)),\\ \dot{\Phi}_2&=-v_u/\varepsilon_D(\rho(\Phi_2)),\end{aligned} \tag{13}$$

and the shock-enhanced stresses

$$\begin{aligned}\sigma_B&=\sigma_0(\rho(\Phi_1))+\rho_f(\Phi_1)(v-v_u)^2/\varepsilon_D(\rho(\Phi_1)),\\ \sigma_b&=\sigma_0(\rho(\Phi_2))+\rho_f(\Phi_2)v_u^2/\varepsilon_D(\rho(\Phi_2)).\end{aligned} \tag{14}$$

The motion of the mass together with the portion behind shock-front 1 is given by

$$\frac{\mathrm{d}v}{\mathrm{d}t}=-\sigma_B\left(m+\int_0^{\Phi_1}\rho_f(X)\,\mathrm{d}X\right)^{-1}. \tag{15}$$

A numerical method is needed to solve these equations with initial conditions $\Phi_1(0)=0$, $\Phi_2(0)=L$, $v(0)=V_0$ and $v_u(0)=0$. At time t_1 corresponding to $v(t_1)=v_u(t_1)$, shock-front 1 ceases. After time t_1, $v_u(t)=v(t)$ and shock-front 2 continues to travel at a speed

$$\dot{\Phi}_2=-v/\varepsilon_D(\rho(\Phi_2)). \tag{16}$$

The motion of mass together with the portion ahead of shock-front 2 is given by

$$\frac{\mathrm{d}v}{\mathrm{d}t}=-\sigma_0(\rho(\Phi_2))\left(m+\int_0^{\Phi_2}\rho_f(X)dX\right)^{-1}. \tag{17}$$

The impact stress is $\sigma_i=-m\,\mathrm{d}v/\,\mathrm{d}t$ and the support stress is $\sigma_s=\sigma_b$. The predicted stresses for $\gamma=-1$ are shown in Fig. 2(b). A jump of the impact stress is predicted at time $t_1=2.63$ ms. Before this time the impact stress drops rapidly, but after that it increases gradually. The support stress increases gradually during the impact process. At time t_{end}, shock-front 2 ceases if the specimen is long enough. However, if the specimen is not long enough, shock-front 2 will propagate to the location of shock-front 1 stopped. This time, t_2, can be determined from $\Phi_2(t_2)=\Phi_1(t_1)$. It is predicted as $t_2=6.17$ ms for $\gamma=-1$. The wave propagation is not considered in the models after the specimen is fully deformed. Results for any $\gamma<0$ can be obtained in a similar way and they are found to have a similar behavior.

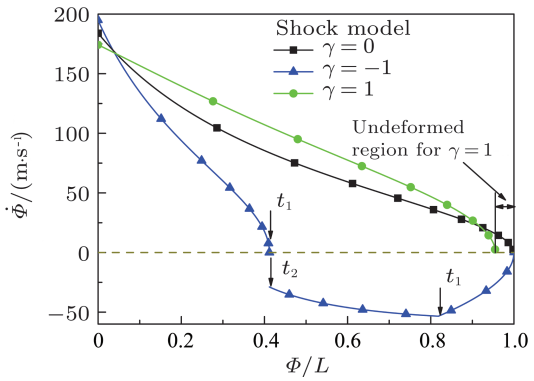

Fig. 3. Predictions of shock speed vs. shock location by the shock models for different density-gradient parameters.

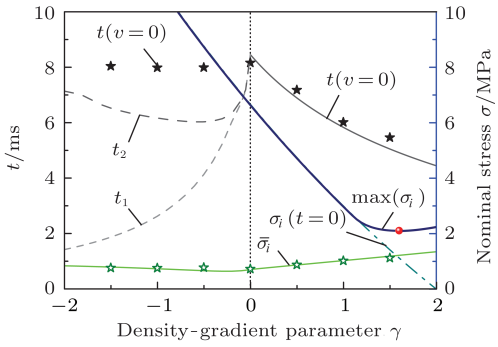

Fig. 4. Variation of impact times and impact stresses (average, maximum and initial) with the density-gradient parameter obtained from the cell-based FE models (plotted with stars) and the shock models (plotted in lines) when $M=5$ g and $V_0=120$ m/s.

The predictions of the impact and support stresses obtained by shock models are compared reasonably well with the FE results. The shock wave propagation mechanisms well explain the deformation and energy absorption processes of GCMs. Figure 3 shows that the shock speeds for $\gamma=0$ and 1 both decrease gradually during the impact process, but for $\gamma=-1$ the situation is much complex: the speed of the shock front close to the impact end drops rapidly, and that close to the support end firstly increases and then decreases gradually. Density gradients affect the propagation of shock waves. For $\gamma=1$, there is an undeformed region when the impact kinetic energy is exhausted. For $\gamma=-1$,

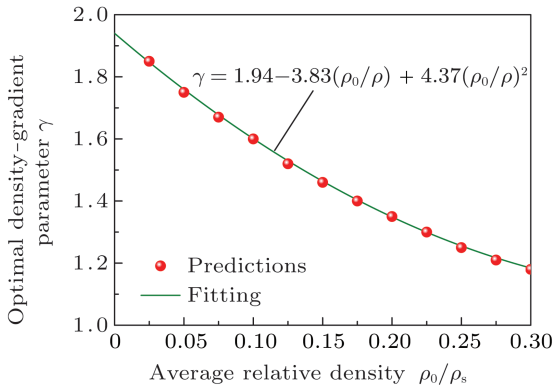

Fig. 5. Optimal density-gradient parameters for different average relative densities of GCMs when $M = 5$ g and $V_0 = 120$ m/s.

the extended shock model predicts that the impact kinetic energy is unexhausted when the specimen is fully deformed. This means that a cellular metal with a positive density gradient may absorb more energy than a uniform cellular metal or a cellular metal with a negative density gradient, and thus Eq. (3) can also be used to obtain a conservative estimation of the length for a GCM rod with an increasing density distribution.

It is wisdom to choose a GCM rod with $\gamma > 0$ to protect the impacting mass, because for this choice the initial impact stress is much small and the impact stress is much stable, see Fig. 2. For $\gamma > 0$, a larger γ leads to a higher level of the average impact stress $\bar{\sigma}_i$ and thus a shorter impact time, as shown in Fig. 4. It is worth to point that, when taking $\gamma = 1.6$, the maximum impact stress, $\max(\sigma_i)$, reaches a minimum value (2.11 MPa), see Fig. 4. Thus, there is an optimal value for the density-gradient parameter γ to meet the crashworthiness requirements of high energy absorption, stable impact resistance and low peak stress. For the case of $M = 5$ g and $V_0 = 120$ m/s considered, the optimal density-gradient parameter decreases with the increase of the average relative density of a GCM rod, as shown in Fig. 5.

A crashworthiness design of cellular metals with a linear density gradient was presented in this paper. Cell-based FE models and extended shock models were employed to study the crashworthiness of GCMs. Introducing a density gradient to cellular metals helps to meet the requirements of crashworthiness. The shock wave propagation mechanisms of GCMs can provide an insight into crashworthiness and other energy absorption structures for applications.

This work was supported by the National Natural Science Foundation of China (90916026, 11002140) and the Fundamental Research Funds for the Central Universities (WK2090050023).

1. G. W. Ma, and Z. Q. Ye, Int. J. Impact Eng. **34**, 329 (2007).
2. G. S. Langdon, D. Karagiozova, and M. D. Theobald, et al., Int. J. Impact Eng. **37**, 638 (2010).
3. L. J. Gibson, and M. F. Ashby, *Cellular Solids: Structures and Properties* (Cambridge University Press, Cambridge, 1997).
4. S. R. Reid, and C. Peng, Int. J. Impact Eng. **19**, 531 (1997).
5. P. J. Tan, S. R. Reid, and J. J. Harrigan, et al., J. Mech. Phys. Solids **53**, 2206 (2005).
6. Z. J. Zheng, Y. D. Liu, and J. L. Yu, et al., Int. J. Impact Eng. **42**, 66 (2012).
7. Z. J. Zheng, J. L. Yu, and C. F. Wang, et al., Int. J. Impact Eng. **53**, 29 (2013).
8. X. K. Wang, Z. J. Zheng, and J. L. Yu, et al., Appl. Mech. Mater. **69**, 73 (2011).
9. H. B. Zeng, S. Pattofatto, and H. Zhao, et al., Int. J. Mech. Sci. **52**, 680 (2010).
10. A. H. Brothers, and D. C. Dunand, Adv. Eng. Mater. **8**, 805 (2006).
11. Y. Hangai, K. Takahashi, and T. Utsunomiya, et al., Mater. Sci. Eng. A **534**, 716 (2012).
12. H. F. Yin, G. L. Wen, and S. J. Hou, et al., Mater. Des. **32**, 4449 (2011).
13. Z. J. Zheng, J. L. Yu, and J. R. Li, Int. J. Impact Eng. **32**, 650 (2005).
14. C. J. Shen, T. X. Yu, and G. Lu, Int. J. Solids Struct. **50**, 217 (2013).